# NIR-Responsive Carbon Nitride of Five-Membered Rings ($C_3N_2$) for Photoelectrochemical Biosensing

Hong Yang, Qing Zhou, Zhengzou Fang, Lufang Zhao, Jin Ma, Wang Li, Songqin Liu, Yanfei Shen, Yuanjian Zhang*

School of Chemistry and Chemical Engineering, Medical School, Jiangsu Engineering Laboratory of Smart Carbon-Rich Materials and Device, Jiangsu Province Hi-Tech Key Laboratory for Bio Medical Research, Southeast University, Nanjing 211189, China, E-mail: Yuanjian.Zhang@seu.edu.cn

Abstract

Polymeric carbon nitrides (pCN) have garnered immense attention, ranging from super-hard materials to artificial photosynthesis, due to their exceptional chemical and optoelectronic properties. The most studied $C_3N_4$ along with other stoichiometric pCN, such as $C_3N$, $C_2N$ and $C_3N_5$, commonly employed a six-membered ring as the basic units; while the five-membered rings are also popular in a myriad of natural and artificial molecules with a more polarized framework and intriguing functionalities. Here, we report a facile synthesis of $C_3N_2$ with a topological structure of five-membered rings, endowing by far the narrowest the first electronic transition energy (0.81 eV) in pCN family. The basic imidazole unit with dangling bonds, resulting in an unusual electronic band of p-π conjugation and split molecular orbitals, was revealed in $C_3N_2$ by both experiments and density functional theory calculations. Moreover, a NIR-responsive photoelectrochemical (PEC) biosensor for non-transparent biosamples was constructed for the first time using $C_3N_2$ with outstanding performance. This work would not only open a new vista of pCN with different topological structures but also broaden the horizon of their application, such as prospective *in vivo* PEC bioassay.

## Introduction

As a metal-free and light-active material, polymeric carbon nitride (pCN) has garnered enormous interest. From the structural view of point, it can be regarded as a graphene analogue, with some C atoms replaced by N atoms in a regular manner.[1] Strikingly, the N dopants in the 2D framework greatly enriches the features of carbon materials, endowing not only unique surface properties but also attractive electronic structures capable of photo-electron interconversion.[2] To this end, pCN has demonstrated a large variety of prospective applications, ranging from photocatalytic water splitting[3], $CO_2$ reduction[4] and oxidation of several small organic molecules[5] to photoelectrochemical (PEC)[6] and electrochemiluminescence (ECL)[7] bioassay. The added advantages include the abundance of sources, the simplicity of synthesis, and high biocompatibility.[8] Notably, the most studied $C_3N_4$ along with other stoichiometric pCN, such as $C_3N$, $C_2N$ and $C_3N_5$,[9] commonly employed a six-membered ring as the periodic repeating units. In contrast, the covalently bonded -C-N- with a topological structure of five-membered rings is also popular in a myriad of natural and artificial important molecules, such as chlorophyll, sedatives, and some homogeneous catalysts (**Figure S1**), enabling more intriguing functionalities for many energy-, signaling- and molecule-conversion processes.[10] Moreover, in principle, the main component of highest occupied molecular orbital (HOMO) of six-membered and five-membered pCN monomer are non-bonding n orbital and bonding π orbital, respectively, endowing the latter more easily to be polarized and obtain higher reactivity (**Figure 1a**). These intriguing facts inspire us that pCN materials consisted of five-membered rings would provide broader perspectives for electronic structure modulation.

However, the synthesis of pCN materials consisted of five-membered rings is rarely explored, presumably owing to the grand challenge of the thermodynamics limitations. On the one hand, the pCN precursors of five-membered ring, such as pyrrole, imidazole, and triazole are volatile organic compounds, which generally evaporated at 200-300 °C, lower than the critical temperature that was required for intermolecular condensation

(e.g. 550 ºC for $C_3N_4$).[11] On the other hand, at higher temperature, the small molecular fragments tend to graphitized into a six-membered ring structure instead of the five-membered one for lower energy.[12]

Here, we report a facile way to synthesize $C_3N_2$ with a five-membered ring by direct condensation of pre-stabilized 2-methylimidazole monomers (2-MIm) in abundant-available metal organic frameworks (MOF). Thanks to the lower energy π→π* electron transition and the abundant dangling bonds in the new topological structure, the first electronic transition energy of the as-prepared $C_3N_2$ was surprisingly reduced to as low as 0.81 eV, the narrowest one in the pCN family to our knowledge. Moreover, $C_3N_2$ demonstrated a remarkable photocurrent in aqueous electrolytes under infrared light irradiation, compared to the most studied $C_3N_4$, and had good biocompatibility. As the very few successful PEC sensing systems responsive to long-wavelength light, $C_3N_2$ photoelectrode was for the first time applied to the non-transparent biologic samples detection in which the visible light could hardly pass through, a sort of first step toward future *in vivo* applications.

**Results and Discussion**

Following the lowest-energy principle, the possible bonding modes for 2-MIm at 298.15 K were firstly explored by using density functional theory (DFT) and shown in **Figure 1b**. The thermodynamic polymerization of two 2-MIm molecules was supposed to be a condensed reaction via a demethylation process at 4'-C and 5'-C sites, due to the steric hindrance effect. The Gibbs free energy change (ΔG) for producing dimer (M2 fragment, a suitable structure, the other three isomers were discussed in **Figure S2**) was -26.6 kJ/mol, indicating the condensation was a spontaneous exothermic process. Interestingly, the formation of a trimer (M1) was more favorable in thermodynamic, considering the ΔG of per covalent linkage, due to the larger conjugation. Four 2-MIm molecules may also polymerize into a ring structure, i.e. M3 fragment, similar to a porphyrin molecule.[14] Although it was endothermic, the reaction generated a large amount of volatile $H_2$, endowing the forward reaction allowed via a proper heating. In

this context, the inter-condensation between 2-MIm was thermodynamically permissible in several different manners.

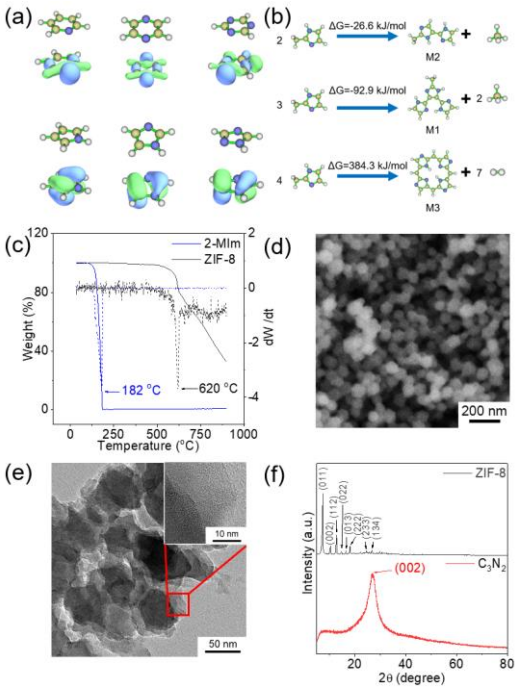


**Figure 1. Synthesis principle and texture of $C_3N_2$.** (a) Topology structure and HOMO of six-/five-membered aromatic pCN monomers. Yellow coloring indicates carbon atoms, blue nitrogen and white hydrogen. Green and blue parts correspond to positive and negative regions, respectively.[13] (b) Polymerization thermodynamics of 2-MIm oligomers by calculation. (c) TGA and DTG curves of 2-MIm and ZIF-8 in $N_2$. (d) SEM and (e) TEM images of $C_3N_2$. The inset showed HR-TEM image. (f) XRD patterns of ZIF-8 and $C_3N_2$.

Nonetheless, 2-MIm completely volatilized at ca. 195 ℃ because of the collapse of the whole crystal structure. Interestingly, when 2-MIm was coordinated to metal ions as a ligand, such as $Zn^{2+}$ into a zeolitic imidazolate framework (ZIF-8), its thermal stability was surprisingly improved. As shown in the thermal gravimetric analysis (TGA, **Figure 1c**), the maximum mass loss temperature of 2-MIm was boosted from 182 ℃ in the monomer to 620 ℃ in the ZIF-8, presumably attributing to the strong complexation and the highly ordered structure.[11a] A second lower mass-loss rate was exclusively observed for ZIF-8, a strong evidence of the thermal condensation of pCN, followed by a further decomposition at an elevated temperature. Thus, in this study, $C_3N_2$ was synthesized by calcining ZIF-8 at 600 ℃. To remove ZnO and other

impurities, the final carbonized product was treated with concentrated hydrochloric acid for 24 h with the content of Zn less than 0.2 at.% (**Table S1**, **S2**).

The morphology of ZIF-8 and as-prepared $C_3N_2$ nanoparticles were determined using scanning electron microscopy (SEM) and transmission electron microscope (TEM). As illustrated in **Figure 1d**, $C_3N_2$ nanoparticles with sizes of 50-70 nm were observed in the SEM image, which largely retained that of the dodecahedron ZIF-8 (**Figure S4**). Nonetheless, some deformation was also noticed in the TEM images (**Figure 1e**), presumably attributing to high-temperature treatment. No apparent lattice fringes were surveyed in the high-resolution TEM image (**Figure 1e, inset**), disclosing a disordered texture. The X-ray diffraction (XRD) pattern of $C_3N_2$ further disclosed a broad peak at $2\theta$ values of 26.9°, corresponding to the (002) diffraction peak with a 0.33 nm interplanar *d*-spacing, which was distinct to that of ZIF-8 (**Figure 1f**).[11a] Notably, ZnO phase was not observed in the final $C_3N_2$ by all of these SEM, TEM (**Figure S5**) and XRD (**Figure S6**) measurements. The $N_2$ adsorption-desorption isotherms gave more information of the porosity (**Figure S7**). Barrett-Joyner-Halenda pore analysis showed compared with ZIF-8 the pore size of $C_3N_2$ was significantly increased, meanwhile the pore volume greatly shrank, so did the surface area, consistent with the tendency of forming a graphitic structure.[15]

The combustion elemental analysis of the as-prepared $C_3N_2$ gave a stoichiometric chemical formula of $C_{3.06}N_2H_{1.79}$ (**Table S3**), which was equivalent to that with the loss of methyl group and Zn from the precursor ZIF-8, with some additional compensation of H atoms. Three possible polymeric units inferring from the imidazole ring were united and shown in **Figure 2a**. Notably, some N atoms (orange) in $C_3N_2$ were in the dangling state,[16] i.e. the unpaired electron (black dot) occupied the $2p_z$ orbital, which will be discussed in details later. To verify the assumed chemical structure of $C_3N_2$, the X-ray photoelectron spectrum (XPS) was firstly measured. **Figure 2b** shows the high-resolution $C_{1s}$ XPS spectrum of $C_3N_2$, which was deconvolved into four peak components of C-C and C=C, C-NH, C-N and C=N at binding energies of 284.4, 285.4,

286.5 and 288.0 eV, respectively.[17] High-resolution $N_{1s}$ XPS spectrum (**Figure 2c**) exhibited two peaks at 398.1 and 399.7 eV, corresponding to C=N-C and C-NH-C, respectively.[15a] Notably, there was no clear peaks corresponding to oxidation of C and N. High-resolution XPS spectra for O and trace Zn were also explored, confirming that they were attribute to the very few residual ZnO and adsorbed water (**Figure S8**).

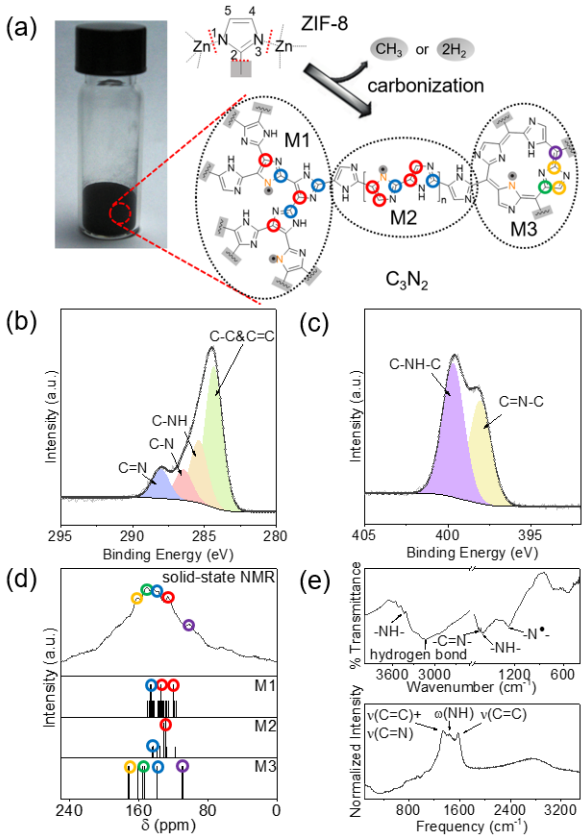


**Figure 2. Molecular structure of $C_3N_2$.** (a) Photo of $C_3N_2$ powders and the typical structures. High resolution (b) C 1s and (c) N 1s XPS spectra of $C_3N_2$. (d) Solid-state $^{13}C$ NMR spectrum of $C_3N_2$ and $^{13}C$ NMR spectrum of the three molecular repeating fragments of $C_3N_2$ by calculation. (e) FT-IR (top panel) and Raman (bottom panel) spectra of $C_3N_2$.

The $^{13}C$ solid-state NMR spectrum (**Figure 2d**) of $C_3N_2$ was further explored. A wide chemical shifts ranging from 100 to 180 ppm were observed, indicative of a series of $sp^2$ hybridization carbons (C=N carbon: 161, 151 ppm, C=C carbon: 138-142, 126 and 103 ppm) from different chemical environments.[18] To understand more detailed information, the theoretical simulation was undertaken, showing the chemical shifts of

the C atom for the M1 and M2 fragments were at 115-140 ppm, and that for the M3 fragment appeared at 103, 151, and 161 ppm, strongly supporting the co-existence of three possible polymeric units in **Figure 2a**.

The FTIR spectrum of $C_3N_2$ also showed some useful structural information (**Figure 2e, top panel**). The characteristic broad peak in range of 3000-3400 $cm^{-1}$ was reminiscent of the hydrogen bonding, which may attribute to the -NH- structure. The vibrations at 3517 and 1589 were assigned to the N-H stretch ($\nu_{N-H}$), and another peak at 1629 $cm^{-1}$ could be ascribed to the -C=N- stretch ($\nu_{C=N}$). Meanwhile, $C_3N_2$ exhibited a peak at 1277 $cm^{-1}$, which was usually attributed to a protonated N atom, was more likely corresponded to -$N^{\cdot}$- with an unpaired electron in this material.[9d, 19] Complementarily, the Raman spectrum of the $C_3N_2$ showed two characteristic peaks of carbon materials at 1336 and 1595 $cm^{-1}$ (**Figure 2e, bottom panel**). The D band at 1336 $cm^{-1}$ was assignable to the C=N stretch ($\nu_{C=N}$) and C=C stretch ($\nu_{C=C}$) of defect-induced breathing mode of $sp^2$ rings, and the G band at 1595 $cm^{-1}$ could be ascribed to stretching vibrations C=C ($\nu_{C=C}$) of a graphitic structure.[20] Considering all the evidence, therefore, 2-MIm was well stabilized by the complexation in the ZIF-8 framework as the ligands, and successfully thermally condensed into $C_3N_2$, maintaining the original five-numbered ring structure, most presumably in the united form of M1, M2 and M3.

The band structure of $C_3N_2$ was studied by Mott–Schottky plot (**Figure 3a**) and Kubelka-Munk plots (**Figure 3b**). According to the Mott–Schottky plot, the negative slope of the $C^{-2}$ values indicative of a typical p-type semiconductor, and the flat band position of ca. 1.14 V *vs* Ag/AgCl was determined from the intersection.[21] More interestingly, distinct to most pCN materials, $C_3N_2$ had a wide absorbance in ultraviolet (UV)-visible-near-infrared (NIR) regions (**Figure S9**). An indirect optical gap of 0.81 eV was calculated for $C_3N_2$, the narrowest one in pCN materials to our knowledge. As such, the electronic band structure of was summarized in **Figure 3b inset**. To further evaluate the possible unpaired electrons, the electron spin resonance (ESR) spectra were measured. **Figure 3c** showed a much stronger ESR intensity for $C_3N_2$ than bulk

g-$C_3N_4$ under identical conditions, indicating a significantly larger number of unpaired electrons in the $sp^2$ hybridized aromatic π-system.[16] It was supposed that the N-dangling bonds with unpaired electrons may be formed by the broken of the Zn-N bonds in ZIF-8 without hydrogen atoms paired.

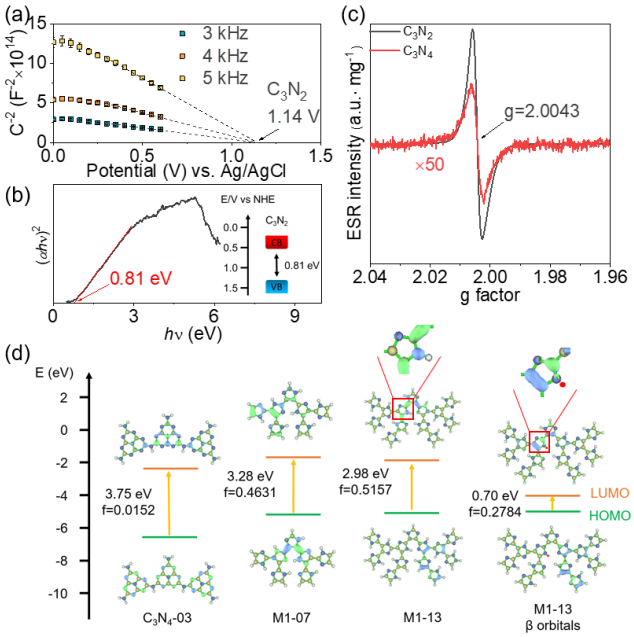


**Figure 3. Electronic band structure of $C_3N_2$.** (a) Mott–Schottky plot of $C_3N_2$ in 0.1 M KCl. (b) Kubelka-Munk plot of $C_3N_2$ powders. The inset shows the calculated electronic band structure of $C_3N_2$. (c) ESR spectrum of $C_3N_2$ and $C_3N_4$. (d) Isosurfaces of the LUMO (top) and HOMO (bottom) of linear $C_3N_4$ and $C_3N_2$ M1 repetitive unit along with the first electronic transition and oscillator strengths (f) by DFT calculations.

As known, the first electronic transition energy without forbidden transition corresponds to the optical gap in value. For a more comprehensive understanding of the contribution of the unique five-numbered ring structure to the unusual narrow optical gap, the DFT calculations of the first electronic transition of linear $C_3N_4$ and $C_3N_2$ were further explored. It was observed that the larger electron delocalization, the narrower the first electronic transition energy for $C_3N_2$ (**Figure S10**). Moreover interestingly, as shown in **Figure 3d**, $C_3N_2$-M1-07 (51 atoms, 240 electrons, 3.28 eV) with less atoms demonstrated a lower transition energy and higher oscillator strengths than $C_3N_4$-03 (65 atoms, 308 electrons, 3.75 eV). It strongly verified the electron transition of π→π* in $C_3N_2$ at the similar scale was easier than that of n→π* in $C_3N_4$.[9a] In fact, some unpaired

electrons also occupied the N $2p_z$ orbitals in $C_3N_2$. Due to the asymmetry of the spin orbitals, the molecular orbitals would split into α orbitals and β orbitals,[22] and the configuration interaction coefficients of the α orbitals were lower than 0.1 in the first three electronic transition (**Table S4**), making the narrow optical gap was mostly depended on β orbitals. As shown in **Figure 3d**, the first electronic transition energy of $C_3N_2$-M1-13 polymerized by 13 imidazole molecules was 2.98 eV, in contrast, the first electronic transition energy of its radical with N-dangling bond was 0.70 eV, well matching the optical gap in experiments. In this context, not only the HOMO and LUMO π orbitals electron delocalization of five-numbered ring but also the N-dangling bonds with unpaired electrons played crucial roles in the unique electronic band structure of $C_3N_2$.

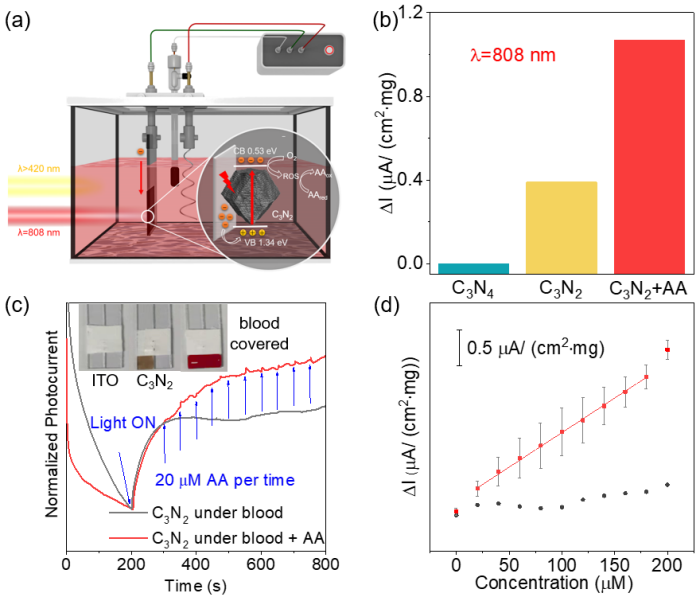


**Figure 4. PEC properties of $C_3N_2$ in non-transparent human whole blood.** (a) Scheme of PEC sensing in human whole blood and the possible charge transfer pathway of photocurrent generation by $C_3N_2$ in the presence of AA. (b) Photocurrent of $C_3N_4$, $C_3N_2$, and $C_3N_2$ measured in human whole blood with 100 μM AA. Biased potential: -0.3 V vs. Ag/AgCl. Non-transparent geometrical light length: 5 mm. (c) Photocurrent and (d) calibration curve of $C_3N_2$ photoelectrode operating on a minimized two-electrode device (inset: photo) containing human whole blood with different concentration of AA.

Thanks to the ultralow band gap, the PEC properties of $C_3N_2$, especially under the

irradiation of near-infrared light regions for non-transparent biological samples, would appeal for more attractive applications. In the first set of experiments, the photocurrent in 0.1 M KCl aqueous solution under the visible light irradiation ($\lambda$>420 nm) was evaluated. **Figure S11** showed that the photocurrent of $C_3N_4$ ($E_g$=2.67 eV) was 1.95 $\mu A \cdot cm^{-2} \cdot mg^{-1}$, while that of $C_3N_2$ ($E_g$=0.81 eV) was boosted more than 10 times reaching 23.22 $\mu A \cdot cm^{-2} \cdot mg^{-1}$ at -0.3 V, strongly demonstrated the importance of narrow band gap in absorption of more light for enhancing photocurrents. Under the 808 nm laser irradiation, bulk $C_3N_4$ cannot be excited at all and the photocurrent became negligible; in contrast, that of $C_3N_2$ could still attain 4.28 $\mu A \cdot cm^{-2} \cdot mg^{-1}$. More interestingly, after replacing the transparent KCl aqueous solution with the non-transparent human whole blood (**Figure 4a,** the geometrical light length: 5 mm), a significant photocurrent of ca. 0.39 $\mu A \cdot cm^{-2} \cdot mg^{-1}$ was still retained (**Figure 4b**).

As an important electron donor or catalyst for alleviation of oxidative stress and biosynthesis *in vivo* such as producing neurotransmitters, ascorbic acid (AA) exists in a diverse of complex biological environments, making the real-time accurate anti-interferent biosensing highly envisioned.[23] In this sense, for the principle verification, 100 μM AA was further added in the blood and the photocurrent was measured under irradiation of 808 nm laser. Interestingly, the photocurrent evidently increased 274% to 1.07 $\mu A \cdot cm^{-2} \cdot mg^{-1}$ (**Figure 4b**), as a result of an accelerated photoreduction of molecular oxygen at $C_3N_2$ photoelectrode driven by AA (**Figure S12 and 4a inset**).[24] Therefore, these results evidently manifested the feasibility of PEC sensing by using $C_3N_2$ photoelectrode in non-transparent biological samples using near-infrared light irradiation.

To facilitate the practical application, a minimized two-electrode device, consisting of a $C_3N_2$-modificed ITO as the working electrode and another ITO as the counter/semi-reference electrodes, was further proposed to monitor the AA concentration in human whole blood in real time. As shown in **Figure 4c**, **d**, compared to the blank control, the boosted photocurrent was linear to the concentration of exogenous AA ranging from 20

μM to 180 μM, with a limit of detection (LOD, 3σ/S) of 15.5 μM. Moreover, the calibration curve had an excellent linearity ($R^2$=0.999), indicative of high precision and reliability in continuous monitoring. Lastly but not less important, the biocompatibility of $C_3N_2$ was also evaluated, showing negligible toxicity to the GES-1, B16, and 4T1 cells at reasonable concentrations. These features would principally make $C_3N_2$ photoelectrode meet the critical requirements for disease diagnosis and management.[25] To our knowledge, this is the first time that the PEC biosensing has been successfully applied to non-transparent biological samples. Therefore, as an emerging narrow semiconductor, $C_3N_2$ (**Figure S13**) held a great potential for future real time PEC biosensing *in vivo*.

## Conclusion

In summary, we demonstrated the synthesis of a novel $C_3N_2$ material consisted of five-membered ring by a mild polymerization of imidazolate and broken of Zn-N bonds from the abundantly available ZIF-8 precursor. The unusual topological structure and the unpaired dangling bonds (N $2p_z$ orbitals) in $C_3N_2$ was verified both in experiments and theoretical calculation, which endowed a significantly narrowed the first electronic transition energy to record-level 0.81 eV, in comparison with the mostly studied g-$C_3N_4$ (ca. 2.7 eV). As a proof of concept, the PEC bioassay of non-transparent biological samples was realized for the first time by using the as-prepared $C_3N_2$, thanks to its outstanding NIR-responsibility. This work would open a new era of carbon nitride family that was dominated previously by the topological structure of six-membered rings, enabling more intriguing functionalities, and thus broaden the horizon of their application, such as prospective *in vivo* PEC biosensing for disease diagnosis and management. In addition, the protocol in creating carbon nitrides with new topological structures by delicate stabilization and condensation of the precursors through metal-organic frameworks intermediate not only avoids the harsh experimental conditions (e.g. high pressure) but also tends to scale-up and expands to other stoichiometric carbon nitrides.

## Acknowledgements

This work was supported by the National Natural Science Foundation of China (21775018, 21675022), the Natural Science Foundation of Jiangsu Province (BK20160028), the Open Funds of the State Key Laboratory of Electroanalytical Chemistry (SKLEAC201909), and the Fundamental Research Funds for the Central Universities. We thank Dr. Zhigang Ni (Hangzhou Normal University), Dr. Peng Li (Nanjing University of Aeronautics and Astronautics), Dr. Jun Li (North University of China) and Dr. Tian Lu (Beijing Kein Research Center for Natural Sciences) for help discussion of theoretical calculation.

## Reference

1. (a) Liu, A. Y.; Cohen, M. L., *Science* **1989,** *245* (4920), 841-842; (b) Teter, D. M.; Hemley, R. J., *Science* **1996,** *271* (5245), 53-55.

2. (a) Wang, X.; Li, X.; Zhang, L.; Yoon, Y.; Weber, P. K.; Wang, H.; Guo, J.; Dai, H., *Science* **2009,** *324* (5928), 768-771; (b) Guo, B.; Tian, L.; Xie, W.; Batool, A.; Xie, G.; Xiang, Q.; Jan, S. U.; Boddula, R.; Gong, J. R., *Nano Lett.* **2018,** *18* (9), 5954-5960.

3. (a) Liu, J.; Liu, Y.; Liu, N.; Han, Y.; Zhang, X.; Huang, H.; Lifshitz, Y.; Lee, S.-T.; Zhong, J.; Kang, Z., *Science* **2015,** *347* (6225), 970-974; (b) Godin, R.; Wang, Y.; Zwijnenburg, M. A.; Tang, J.; Durrant, J. R., *J. Am. Chem. Soc.* **2017,** *139* (14), 5216-5224.

4. (a) Gao, G.; Jiao, Y.; Waclawik, E. R.; Du, A., *J. Am. Chem. Soc.* **2016,** *138* (19), 6292-7; (b) Kuriki, R.; Matsunaga, H.; Nakashima, T.; Wada, K.; Yamakata, A.; Ishitani, O.; Maeda, K., *J. Am. Chem. Soc.* **2016,** *138* (15), 5159-70.

5. (a) Wang, Y.; Wang, X.; Antonietti, M., *Angew.Chem. Int. Ed.* **2012,** *51* (1), 68-89; (b) Cao, S.; Low, J.; Yu, J.; Jaroniec, M., *Adv. Mater.* **2015,** *27* (13), 2150-76; (c) Zhao, Y.; Antonietti, M., *Angew.Chem. Int. Ed.* **2017,** *56* (32), 9336-9340.

6. (a) Bard, A. J., *Science* **1980,** *207* (4427), 139-144; (b) Grätzel, M., *Nature* **2001,** *414* (6861), 338-344; (c) Zhang, Y.; Antonietti, M., *Chem. - Asian J.* **2010,** *8*, 1307-1311; (d) Fang, Y.; Xu, Y.; Li, X.; Ma, Y.; Wang, X., *Angew.Chem. Int. Ed.* **2018,** *57* (31), 9749-9753.

7. (a) Wu, P.; Hou, X.; Xu, J. J.; Chen, H. Y., *Chem. Rev.* **2014,** *114* (21), 11027-59; (b) Ji, J.; Wen, J.; Shen, Y.; Lv, Y.; Chen, Y.; Liu, S.; Ma, H.; Zhang, Y., *J. Am. Chem. Soc.* **2017,** *139* (34), 11698-11701; (c) Li, L.; Chen, Y.; Zhu, J. J., *Anal. Chem.* **2017,** *89* (1), 358-371; (d) Lv, Y.; Chen, S.; Shen, Y.; Ji, J.; Zhou, Q.; Liu, S.; Zhang, Y., *J. Am. Chem. Soc.* **2018,** *140* (8), 2801-2804; (e) Zhao, T.; Zhou, Q.; Lv, Y.; Han, D.; Wu, K.; Zhao, L.; Shen, Y.; Liu, S.; Zhang, Y., *Angew.Chem. Int. Ed.* **2020,** *59* (3), 1139-1143.

8. Vilela, F.; Zhang, K.; Antonietti, M., *Energy Environ. Sci.* **2012,** *5* (7), 7819.

9. (a) Wang, X.; Maeda, K.; Thomas, A.; Takanabe, K.; Xin, G.; Carlsson, J. M.; Domen, K.; Antonietti, M., *Nat. Mater.* **2009,** *8* (1), 76-80; (b) Mahmood, J.; Lee, E. K.; Jung, M.; Shin, D.; Choi, H.-J.; Seo, J.-M.; Jung, S.-M.; Kim, D.; Li, F.; Lah, M. S.; Park, N.; Shin, H.-J.; Oh, J. H.; Baek, J.-B., *Proc. Natl.*

*Acad. Sci. U. S. A.* **2016,** *113* (27), 7414-7419; (c) Mahmood, J.; Lee, E. K.; Jung, M.; Shin, D.; Jeon, I. Y.; Jung, S. M.; Choi, H. J.; Seo, J. M.; Bae, S. Y.; Sohn, S. D.; Park, N.; Oh, J. H.; Shin, H. J.; Baek, J. B., *Nat. Commun.* **2015,** *6*, 6486; (d) Kumar, P.; Vahidzadeh, E.; Thakur, U. K.; Kar, P.; Alam, K. M.; Goswami, A.; Mahdi, N.; Cui, K.; Bernard, G. M.; Michaelis, V. K.; Shankar, K., *J. Am. Chem. Soc.* **2019**; (e) Kim, I. Y.; Kim, S.; Jin, X.; Premkumar, S.; Chandra, G.; Lee, N.-S.; Mane, G. P.; Hwang, S.-J.; Umapathy, S.; Vinu, A., *Angew.Chem. Int. Ed.* **2018,** *57* (52), 17135-17140.

10. (a) Genty, B.; Briantais, J.-M.; Baker, N. R., *Biochim. Biophys. Acta* **1989,** *990* (1), 87-92; (b) Griffiths, M. Z.; Popelier, P. L. A., *J. Chem. Inf. Model.* **2013,** *53* (7), 1714-1725.

11. (a) Park, K. S.; Ni, Z.; Cote, A. P.; Choi, J. Y.; Huang, R.; Uribe-Romo, F. J.; Chae, H. K.; O'Keeffe, M.; Yaghi, O. M., *Proc. Natl. Acad. Sci. U. S. A.* **2006,** *103* (27), 10186-10191; (b) Wang, B.; Cote, A. P.; Furukawa, H.; O'Keeffe, M.; Yaghi, O. M., *Nature* **2008,** *453* (7192), 207-11.

12. (a) Peng, G.; Xing, L.; Barrio, J.; Volokh, M.; Shalom, M., *Angew.Chem. Int. Ed.* **2018,** *57* (5), 1186-1192; (b) Zhou, Z.; Zhang, Y.; Shen, Y.; Liu, S.; Zhang, Y., *Chem. Soc. Rev.* **2018**.

13. Lu, T.; Chen, F., *J. Comput. Chem.* **2012,** *33* (5), 580-92.

14. Asano, N.; Uemura, S.; Kinugawa, T.; Akasaka, H.; Mizutani, T., *J. Phys. Chem. C* **2007,** *72* (14), 5320-5326.

15. (a) Wang, S.; Shang, L.; Li, L.; Yu, Y.; Chi, C.; Wang, K.; Zhang, J.; Shi, R.; Shen, H.; Waterhouse, G. I.; Liu, S.; Tian, J.; Zhang, T.; Liu, H., *Adv. Mater.* **2016,** *28* (38), 8379-8387; (b) Xu, B.; Wang, H.; Wang, W.; Gao, L.; Li, S.; Pan, X.; Wang, H.; Yang, H.; Meng, X.; Wu, Q.; Zheng, L.; Chen, S.; Shi, X.; Fan, K.; Yan, X.; Liu, H., *Angew.Chem. Int. Ed.* **2019,** *58* (15), 4911-4916.

16. Zhou, G.; Shan, Y.; Hu, Y.; Xu, X.; Long, L.; Zhang, J.; Dai, J.; Guo, J.; Shen, J.; Li, S.; Liu, L.; Wu, X., *Nat. Commun.* **2018,** *9* (1), 3366.

17. Kou, Y.; Xu, Y.; Guo, Z.; Jiang, D., *Angew.Chem. Int. Ed.* **2011,** *50* (37), 8753-7.

18. (a) Zhao, D.; Dong, C.; Wang, B.; Chen, C.; Huang, Y.; Diao, Z.; Li, S. Z.; Guo, L.; Shen, S., *Adv. Mater.* **2019,** *31* (43), e1903545; (b) Johnson, J. P.; Bringley, D. A.; Wilson, E. E.; Lewis, K. D.; Beck, L. W.; Matzger, A. J., *J. Am. Chem. Soc.* **2003,** *125* (48), 14708-14709; (c) Besley, N. A.; Titman, J. J.; Wright, M. D., *J. Am. Chem. Soc.* **2005,** *127* (50), 17948-17953.

19. (a) Zhou, Z.; Wang, J.; Yu, J.; Shen, Y.; Li, Y.; Liu, A.; Liu, S.; Zhang, Y., *J. Am. Chem. Soc.* **2015,** *137* (6), 2179-82; (b) Landry, V. K.; Minoura, M.; Pang, K.; Buccella, D.; Kelly, B. V.; Parkin, G., *J. Am. Chem. Soc.* **2006,** *128* (38), 12490-12497.

20. (a) Dresselhaus, M. S.; Dresselhaus, G.; Saito, R.; Jorio, A., *Phys. Rep.* **2005,** *409* (2), 47-99; (b) Chen, Y.; Wang, H.; Li, J.; Lockard, J. V., *J. Mater. Chem. A* **2015,** *3* (9), 4945-4953.

21. Rettie, A. J.; Lee, H. C.; Marshall, L. G.; Lin, J. F.; Capan, C.; Lindemuth, J.; McCloy, J. S.; Zhou, J.; Bard, A. J.; Mullins, C. B., *J. Am. Chem. Soc.* **2013,** *135* (30), 11389-96.

22. Kobayashi, Y.; Yoshioka, M.; Saigo, K.; Hashizume, D.; Ogura, T., *J. Am. Chem. Soc.* **2009,** *131* (29), 9995-10002.

23. Cheng, H.; Li, L.; Zhang, M.; Jiang, Y.; Yu, P.; Ma, F.; Mao, L., *TrAC, Trends Anal. Chem.* **2018,** *109*, 247-259.

24. Zhou, Q.; Li, G.; Chen, K.; Yang, H.; Yang, M.; Zhang, Y.; Wan, Y.; Shen, Y.; Zhang, Y., *Anal. Chem.* **2019,** *92* (1), 983-990.

25. Yun, J.; Mullarky, E.; Lu, C.; Bosch, K. N.; Kavalier, A.; Rivera, K.; Roper, J.; Chio, I. I. C.; Giannopoulou, E. G.; Rago, C.; Muley, A.; Asara, J. M.; Paik, J.; Elemento, O.; Chen, Z.; Pappin, D. J.; Dow, L. E.; Papadopoulos, N.; Gross, S. S.; Cantley, L. C., *Science* **2015,** *350* (6266), 1391-1396.